2_C46

A Numerical Study of the Effect of Limited Space Air Stability on SARS-CoV-2 Spreading in a Ventilated Room

Xiaorui Deng, PhD **Guangcai Gong, PhD** **Yanhong Fang**

ABSTRACT

Worldwide concern has been focused on the airborne disease of the COVID-19 pandemic. This study investigated the effect of the limited space air stability on the mechanism of SARS-CoV-2 spreading in the interpersonal breathing microenvironment using an unsteady computational fluid dynamics (CFD) method. A validated numerical model was employed to simulate the transient SARS-CoV-2 releasing process from normal breathing activity. The computational domain was divided into an interpersonal breathing microenvironment and the rest macroenvironment. A displacement ventilation system was implemented with 1.5 ACH, 3 ACH, 7.4 ACH and 9 ACH. Two standing CSPs (Computational Simulated Person) were placed in the middle of the macroenvironment face-to-face with a relative distance of 1 m. Simulation results indicated that in stable cases, the exhaled SARS-CoV-2 tended to accumulate in the interpersonal breathing microenvironment and resulted in a relatively high infection risk for people; whereas in cases where unstable air presented, SARS-CoV-2 concentration was significantly reduced. The unstable conditions lowered the risk of person-to-person transmission in confined spaces. Also, it was found that unstable cases performed better in energy efficiency in comparison with the stable conditions.

INTRODUCTION

Since the outbreak of the severe acute respiratory syndrome (SARS) in 2003, airborne transmission of infectious respiratory disease in limited spaces has received comprehensive studies (Morawska et al. 2009; Seepana and Lai 2012). The most recent COVID-19 pandemic has drawn worldwide concern again on the transmission of infectious disease between people via respiratory activities (Morawska and Cao 2020; Bourouiba 2020). Respiratory activities release large amounts of organic substances into the ambient environment contaminants, and for patients, this process may also include infectious viruses and airborne aerosols, for example, the airborne SARS-CoV-2 (the white lung viruses that can induce white lung). If not being dispersed effectively, these harmful and infectious contaminants might be inhaled by healthy bodies and increase the possibility of being infected. For the sake of occupant health, the number of infectious contaminants should be controlled at an acceptable level in the breathing microenvironment.

Normally, building ventilation methods are implemented to regulate the distribution of contaminant by offering various airflow patterns to the room (Bolashikov and Melikov 2009). However, it is found that it might not be essential in reducing infection risk with only the ventilation system operating in the built environment. Liu et al. (2016) found that the general dilution ventilation method is ineffective for the short-range airborne transmission of contaminants. In some circumstances, displacement ventilation may even put higher infection risks on people (Nielsen et al. 2008). In this regard, advanced

Xiaorui Deng is a PhD in the College of Civil Engineering, Hunan University, Changsha, China, 410082. **Guangcai Gong** is a professor in the College of Civil Engineering, Hunan University, Changsha, China, 410082. Email: gcgong@hnu.edu.cn. **Yanhong Fang** is an associated professor in the College of Environmental Science and Engineering, Hunan University, Changsha, China, 410082.

environmental control systems are in urgent need.

Recent research found that the vertical temperature distribution in the indoor environment would affect the transmission of infectious contaminants in the breathing microenvironment (Gong et al. 2010; Gong and Deng 2017). They classified the air condition in limited spaces by the ratio of the air's buoyancy term to the vertical inertia term. In a stable environment, where the ratio is greater than zero, the exhaled flow tends to retain the initial inertia force and the majority would stay in the mainstream of the exhaled flow. In an unstable environment, where the ratio is smaller than zero, the exhaled air mixes intensely with the ambient turbulent air. It is therefore more likely for the exhaled flow to deviate from the original direction and diffuse to the macroenvironment.

In this numerical study, the objective is to investigate the distribution of exhaled airborne SARS-CoV-2 in the interpersonal breathing microenvironment in a combined environmental control system by applying limited space air stability into a ventilated room. The influence of ventilation rates on the distribution of SARS-CoV-2 aerosols concentration as well as on the infection risk was examined based on the simulation results. The results can further improve the understanding of the transmission mechanism of exhaled airborne SARS-CoV-2 aerosols in the breathing microenvironment between persons.

METHOD

Geometry and grid

Simulations were conducted by computational fluid dynamics (CFD) to obtain the flow field and the distribution of SARS-CoV-2 aerosols in the ventilated room under stable and unstable conditions. As shown in Figure 1a, the dimension of the computational geometry was 4.0 m (length)× 3.9 m (width)× 2.4 m (height), which was in line with our experimental settings (Deng and Gong 2021). Stable and unstable conditions were created by adjusting the temperature of the top and the bottom of the model room. When the temperature gradient was positive, the air environment was in a stable condition; when it was negative, unstable condition. Displacement ventilation was established by a supply inlet placed at the bottom of one sidewall and an exhaust outlet at the top of the opposite wall. Two standing computer manikins (CSPs) with 1.68m height (Bjørn 1999) were placed in the cross-section plane of z = 2.0 m, with a relative distance of 1.0 m, conducting a respiration process by inhaling through the nose and exhaling through the mouth. The diameter of each nostril was 8.0 mm and the opening area size of the mouth was 110.0 mm^2.

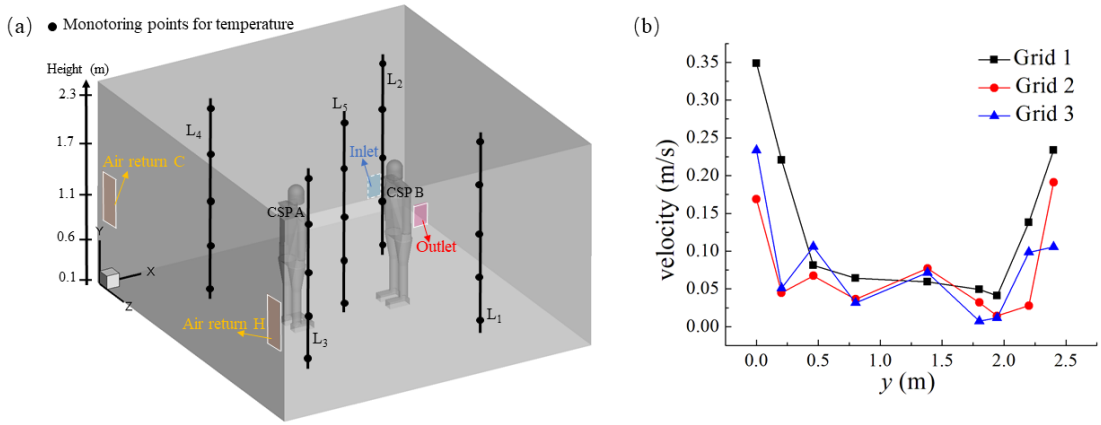

Figure 1 (a) A sketch of relative positions of two CSPs and the monitoring points for temperature. (b) Grid independence test

The computation domain was divided into two parts: two rectangular volumes that surrounding the CSPs and the remained room space. The rectangular volumes were meshed with unstructured cells, and the rest of the room was broken by structured cells. This hybrid method maintained a preferable mesh quality. Grid independence was checked over three grid resolutions: 1,937,399 (Grid 1), 2,324,634 (Grid 2), and 5,551,878 (Grid 3). Comparisons of velocity profile along L5 (Figure 1a) for Grid 1, Grid 2 and Grid 3 are presented in Figure 1b, from which we can see that Grid 2 and Grid 3 exhibited better

grid independences. Considering the computational accuracy and efficiency, Grid 2 was used for further analysis. The vertical temperature was monitored by twenty-five monitor points distributing along five poles (L_1-L_5) at different heights (0.1 m, 0.6 m, 1.1 m, 1.7 m, 2.3 m).

Governing equations

The Reynolds-averaged Navier–Stokes equations were adopted in this study to simulate the airflow. The governing equations are described as follows:

Continuity equation:

$$\frac{\partial \rho}{\partial t} + \nabla \cdot (\rho \boldsymbol{u}) = 0 \tag{1}$$

Momentum equation:

$$\frac{\partial (\rho \boldsymbol{u})}{\partial t} + \mathrm{div}(\rho \boldsymbol{u}\boldsymbol{u}) = \frac{\partial p}{\partial x_i} + \mathrm{div}(\mu \mathrm{grad} u) + \mathrm{S_M} \tag{2}$$

Energy equation:

$$\frac{\partial (\rho T)}{\partial t} + \mathrm{div}(\rho T \boldsymbol{u}) = \rho \mathrm{div}\boldsymbol{u} + \mathrm{div}(k \times \mathrm{grad} T) + \mathrm{S_T} \tag{3}$$

Species:

$$\frac{\partial (\rho \varphi)}{\partial \mathrm{t}} + \mathrm{div}(\rho \varphi \boldsymbol{u}) = \rho \mathrm{div}\boldsymbol{u} + \mathrm{div}(\Gamma_\varphi \times \mathrm{grad}\varphi) + \mathrm{S_\varphi} \tag{4}$$

Where t is the time (sec), ρ is the air density (kg/m^3), $\boldsymbol{u}$ is the velocity vector (m/s), μ is the dynamic viscosity (kg/m·s), p is the pressure (Pa), k is the heat transfer coefficient (W/m·J), T is the temperature (K), φ is the tracer gas concentration, Γ_φ is the diffusion coefficient (m^2/s), and S_M, S_T, and S_φ are the source terms.

Boundary conditions

The supply flow entered the room through the supply inlet at 25℃, providing a ventilation rate of 1.5 ACH, 3 ACH, 7.4 ACH and 9 ACH, respectively. The boundary condition for the exhaust outlet was a pressure-outlet. Based on the experimental settings, two air returns were used alternatively. When the model room was in a stable condition, air return H was applied with a pressure-outlet condition and air return C was regarded as the wall boundary; when the model room was in a stable condition, air return C was applied with the pressure-outlet condition and air return H was regarded as the wall boundary. This arrangement of air return was in accordance with the experimental setting, which can be found in Deng and Gong (2021). The sidewalls of the test room were well-insulated and can be considered adiabatic. The temperature for the ceiling and the floor were 26℃, 21℃ for stable conditions and 25.5℃, 33℃ for unstable conditions. The temperature of the exhalation flow and the CSP surface temperature was 34℃ (Villafruela et al. 2016; Seepana and Lai 2012). A sinusoidal function was used to simulate the breathing process (Villafruela et al. 2013). The sinusoidal function was applied to the mouth and nose boundary conditions by a user-defined function (UDF).

Tracer gas was used to simulate the transport of exhaled airborne SARS-CoV-2-laden aerosols. The reasons for using tracer gas as the surrogate of exhaled SARS-CoV-2-laden aerosols are listed as following. First, according to the Reynolds analogy (Reynolds 1961; Silver 1950) and the extended Reynolds analogy (Hinze 1987; Gong and Deng 2017), the mechanism of heat and mass transfer and shear stress for incompressible flows shared similar characteristics, therefore, it is expected that gas and particulate transport process can be treated as a continuum. Further, the submicron region of the diameter of aerosols with SARS-CoV-2 dominates from 0.25 to 1.0 μm, which makes the aerosols normally do not settle (Tellier 2006) and remain airborne in the built environment (Morawska and Cao 2020). Based on the above reasons, we believe that the tracer gas is a suitable substitute to simulate the commonest range of expiratory airborne SARS-CoV-2-laden aerosols. Rudnick and Milton (2003) proposed a CO_2-based risk equation based on the Wells-Riley equation, which allows one to estimate the risk of the airborne transmission of viruses in limited spaces according to different CO_2 values indoors,

thus we chose CO_2 as the tracer gas in this study. The volume of exhaled air during breathing is assumed to be 12 l/min (Gupta et al., 2010). The exhaled concentration of CO_2 from the mouths was 45 000 ppm (Berlanga et al. 2017) and from the supply inlet was 440 ppm (Deng and Gong 2021).

Turbulent models

Most Reynolds averaged Navier-Stokes (RANS) models are computationally economic and provide useful results. Among the RANS models, the *k-ε* models show the best overall performance compared to other models in terms of accuracy, computing efficiency and robustness (Launder and Spalding, 1974), thus RNG *k-ε* model was selected to calculate the flow filed in the model room along with the enhanced wall treatment. The SIMPLEC (Semi-Implicit Method for Pressure - Linked Equations - Consistent) velocity - pressure coupling algorithm and the second-order upwind spatial discretisation scheme were used to solve the momentum, turbulent kinetic energy, turbulent dissipation rate and tracer gas diffusion for steady and transient computations. The initial conditions for the transient calculations were obtained from a converged steady simulation. During the transient simulation, the time step size was 0.01 secs and each case was simulated for 60 secs (including 16 breathing cycles). All together 8 cases were investigated (Table 1).

Table 1. Detail of case settings

Cases	Case 1	Case 2	Case 3	Case 4	Case 5	Case 6	Case 7	Case 8
Limited space air stability conditions	stable	unstable	stable	unstable	stable	unstable	stable	unstable
Ventilation rates (ACH)	1.5	1.5	3.0	3.0	7.4	7.4	9.0	9.0

RESULTS AND DISCUSSION

Validation of the numerical model

Comparison between numerical results and experimental measurements of vertical temperature profiles in the unstable case is shown in Figure 2. The ventilation rate was 9 ACH. The results for simulation and the experiments showed a similar tendency, with the average discrepancy between numerical results and experimental results 1.01 %. The discrepancy was in an acceptable range (Mendez et al. 2008), thus the established numerical model was used to predict the flow field and the distribution of contaminant in the breathing microenvironment.

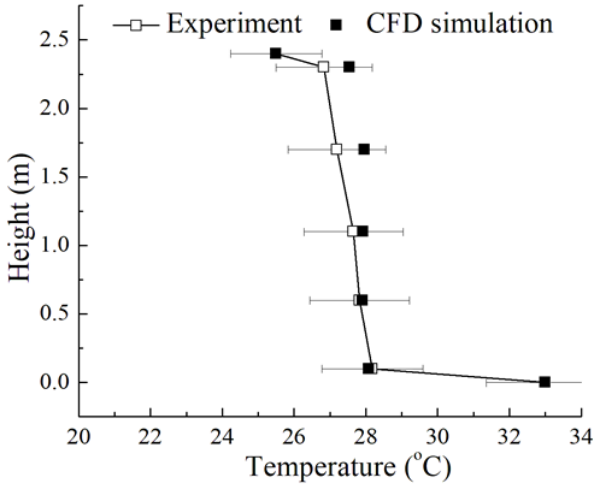

Figure 2 Comparison of the numerical results and the experimental measurements of an unstable case.

Concentration distribution in stable and unstable cases

The distribution of the concentration of exhaled SARS-CoV-2-laden aerosols was obtained by releasing the buoyant tracer gas CO_2 from the mouths of CSP A and CSP B simultaneously. The concentration (C) was normalized by $(C_i\text{-}C_b)/C_b$, where C_i was the contaminant concentration in the measuring point of the interpersonal breathing microenvironment, ppm; C_b was the background concentration of the contaminants, ppm. Figure 3 illustrates the contours of normalized concentration of the simulated cases. As the temperature of the exhalation flow was higher than that of the ambient air, a fraction of the SARS-CoV-2-laden aerosols near the periphery of the exhalation mainstream diffused beyond the upper interpersonal breathing microenvironment due to the buoyance effect.

For the unstable case, when the ventilation rate was relatively low at 1.5 ACH and 3.0 ACH (Figures 3b and 3d), the distributions of the exhaled SARS-CoV-2-laden aerosols mainly concentrated in the upper part of the model room, however, the concentration in the breathing microenvironment was lower than that of the stable counterparts (Figures 3a and 3c), where two exhalation flows from CSP A and CSP B penetrated horizontally towards each other and remarkably reinforced in the middle of the breathing microenvironment. This was due to that the stable temperature stratifications associated with the stable conditions as well as the displacement ventilation system inserted a confinement effect on the exhaled aerosols so that most of the aerosols accumulated in the breathing microenvironment. In such a heavily contaminated breathing microenvironment people have a higher possibility of being infected by an infectious coronavirus.

As the ventilation rate increased to 7.4 ACH and 9.0 ACH, exhaled SARS-CoV-2-laden aerosols of the unstable cases (Figures 3e and 3h) deviated from the mainstream direction soon after they were expelled from the mouth, and the concentration level of $C = 0.01$ expanded to the entire room, thus the infection risk was greatly reduced due to the dilution by ambient air. This was mainly because that the negative temperature gradients resulted from the unstable condition caused instability to the flow field in the model room, which disturbed the stratification associated with the displacement ventilation system and produced a well-mixed interior that further reduced SARS-CoV-2-laden aerosols stratification in the room (Causone et al. 2010). Compared with unstable cases, the transport of the exhaled aerosols in stable cases (Figures 3f and 3g) seemed rather inert to the increase of ventilation rate. The distribution of the SARS-CoV-2-laden aerosols remained suspended in the breathing microenvironment in a way that is shown in Figures 3a and 3c. This is because the stable case presented a more stably stratified temperature field, so the flow field was less likely to be affected by increasing the ventilation rate. As a result, when the ventilation rate increased, most of the exhaled SARS-CoV-2-laden aerosols remained in the interpersonal breathing microenvironment, resulting in relatively high infection risk. It should be noted that though the SARS-CoV-2-laden aerosols distributed to a larger area in unstable cases than in stable cases, the concentration in the breathing microenvironment was smaller. This indicated that increasing ventilation rate of stable air environments may not achieve as good contaminant removal efficiency as that of unstable air environments while consumes the same amount of building energy.

CONCLUSION

The present study provides a numerical analysis of the exhaled airborne contaminant distribution and the thermal field in the interpersonal breathing microenvironment in a ventilated room with stable and unstable conditions. The results obtained for vertical temperature profiles indicated reasonably good agreement between numerical predictions and experimental measurements. The following conclusions are made.

In unstable conditions, the exhaled SARS-CoV-2-laden aerosols were more likely to deviate from their mainstream direction and resulted in a uniform distribution of contaminant in the macroenvironment. The infection risk in the interpersonal breathing microenvironment was, therefore, lower than that of stable conditions. Stable conditions would enhance the stable stratifications of a displacement ventilation, as a result, the exhaled SARS-CoV-2-laden aerosols were more likely to be confined in the interpersonal breathing microenvironment and thus caused high infection risks for the persons nearby. Unstable conditions provided a fully mixed temperature field and worked energy-efficient in removing the exhaled SARS-CoV-2-laden aerosols from the interpersonal breathing microenvironment and reducing the risk of cross-infection between people.

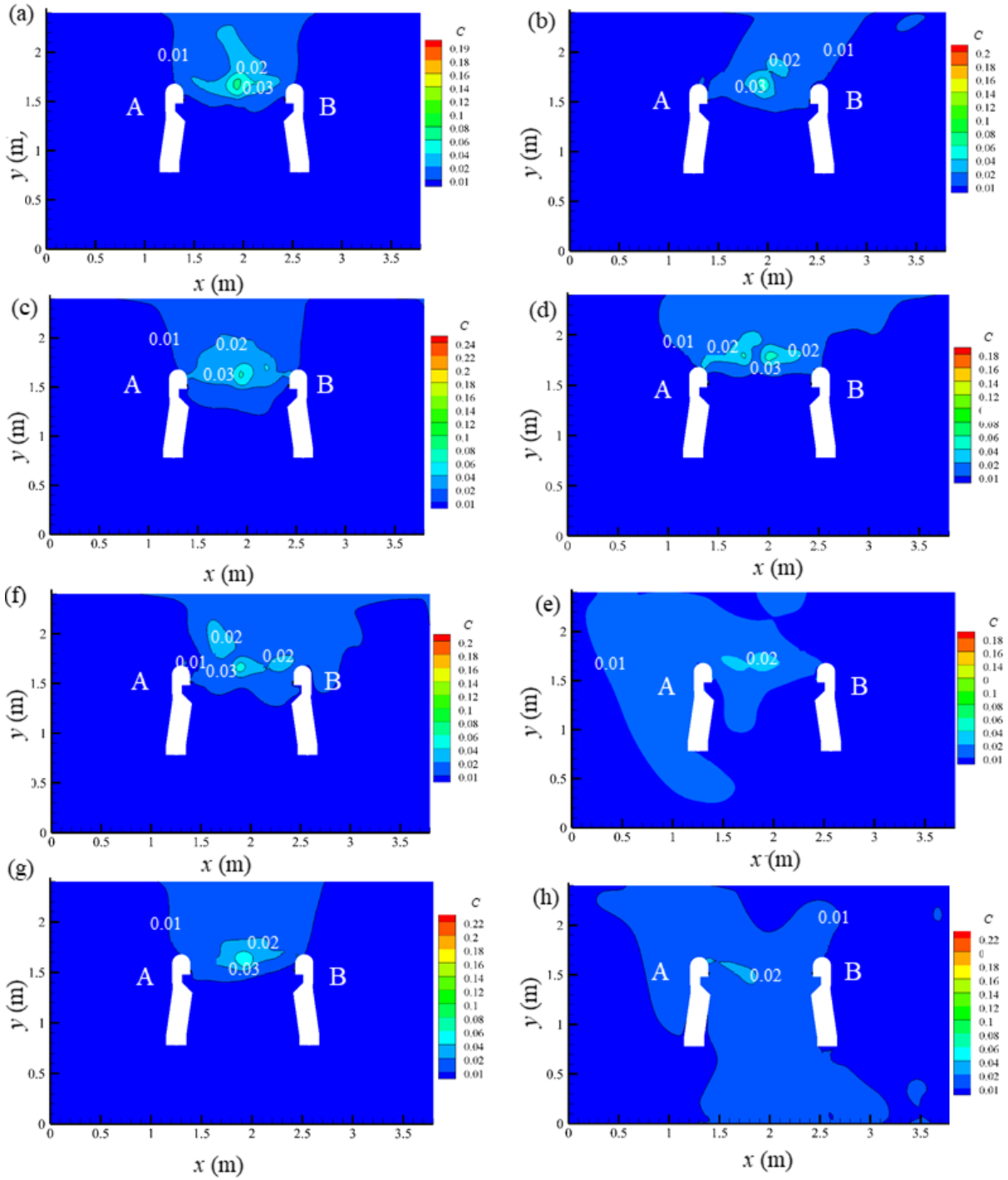

Figure 3 Distribution of exhaled airborne SARS-CoV-2 aerosols at the cross section of z = 2.00 m when t = 35 s, (a) Case 1, (b) Case 2, (c) Case 3, (d) Case 4, (e) Case 5, (f) Case 6, (g) Case 7, (h) Case 8. A (CSP A) and B (CSP B).

ACKNOWLEDGMENTS

This study was funded by the National Natural Science Foundation of China (No.51378186) and the National Science & Technology Supporting Program (No.2015BAJ03B00). The authors acknowledge financial support from the China Scholarship Council at the University of Cambridge (No. 201806130150).

REFERENCES

Berlanga, F.A., Olmedo, I., and M. Ruiz de Adana. 2017. Experimental analysis of the air velocity and contaminant dispersion of human exhalation flows. *Indoor Air* 27: 803-815.

Bolashikov, Z.D., and A.K. Melikov. 2009. Methods for air cleaning and protection of building occupants from airborne pathogens. *Building and Environment* 44:1378–1385.

Bourouiba, L. 2020. Turbulent gas clouds and respiratory pathogen emissions: potential implications for reducing transmission of COVID-19. *The Journal of the American Medical Association* 323(18):1837–1838.

Causone, F., Olesen, B.W., and S.P. Corgnatia. 2010. Floor heating with displacement ventilation: an experimental and numerical analysis. *HVAC&R. Research* 16:139-160.

Deng, X., Gong G, He X, Shi X, and L. Mo. 2021. Control of exhaled SARS-CoV-2-laden aerosols in the interpersonal breathing microenvironment in a ventilated room with limited space air stability. *Journal of Environmental Sciences* 108: 175–187.

Gong, G., Han, B., Luo, H., Xu, C., and K. Li. 2010. Research on the air stability of limited space. *International Journal of Green Energy* 7: 43-64.

Gong, G., and X. Deng. 2017. Nature and characteristics of temperature background effect for interactive respiration process. *Scientific Reports* 7:1-8.

Hinze, J.O. 1987. Turbulence, McGraw-Hill Book Company Inc., New York, pp. 372–416.

Launder, B., and D. Spalding. 1974. The numerical computation of turbulent flows. *Computer Methods in Applied Mechanics and Engineering* 3: 269-289.

Liu L., Li Y., Nielsen P.V., Wei, J., and R.L. Jensen. 2016. Short- range airborne transmission of expiratory droplets between two people. *Indoor Air* 27: 452–462.

Mendez, C., San Jose, J.F., Villafruela, J. M., and F. Castro. 2008. Optimization of a hospital room by means of CFD for more efficient ventilation. *Energy and Buildings* 40: 849–854.

Morawska, L., Johnson, G., Ristovski, Z., Hargreaves, M., Mengersen, K., and S. Corbett. 2009. Size distribution and sites of origin of droplets expelled from the human respiratory tract during expiratory activities. *Journal of Aerosol Science* 40: 256–269.

Morawska, L., and J. Cao. 2020. Airborne transmission of SARS-CoV-2: The world should face the reality. *Environment International* 139: 105730.

Nielsen, P.V., Winther, F.V., Buus, M., and M. Thilageswaran. 2008. Contaminant flow in the microenvironment between people under different ventilation conditions. *ASHRAE Transactions* 114(2): 632-638.

Reynolds, O. 1961. On the extent and action of the heating surface of steam boilers. *International Journal of Heat and Mass Transfer* 3(2): 163–166.

Rudnick, S.N. and D.K. Milton. 2003. Risk of indoor airborne infection transmission estimated from carbon dioxide concentration. *Indoor Air* 13: 237–245

Seepana, S., and A.C.K. Lai. 2012. Experimental and numerical investigation of interpersonal exposure of sneezing in a full-scale chamber. *Aerosol Science and Technology* 46: 485-493.

Silver, R.S. 1950. Application of the reynolds analogy to combustion of solid fuels. *Nature* 165: 725–726.

Tellier, R. 2006. Review of aerosol transmission of influenza A virus. *Emerging Infectious Diseases* 12: 1657–1662.

Villafruela, J.M., Olmedo, I., and J.F. San Jose. 2016. Influence of human breathing modes on airborne cross infection risk. *Building and Environment* 106: 340-351.

Villafruela, J.M., Olmedo, I., Ruiz de Adana, M., Méndez, C., and P.V. Nielsen. 2013. CFD analysis of the human exhalation flow using different boundary conditions and ventilation strategies. *Building and Environment* 62: 191-200

Xu, C., and L. Liu. 2018. Personalized ventilation: One possible solution for airborne infection control in highly occupied space? Indoor. *Building and Environment* 27: 873-876.